Quantification of High Temperature Transition Al_2O_3 and Their Phase Transformations

Libor Kovarik[1*], Mark Bowden[2*], Amity Andersen[2], Nicholas R. Jaegers[1], Nancy Washton[1,2], Janos Szanyi[1]

[1] Institute for Integrated Catalysis, Pacific Northwest National Laboratory, P.O. Box 999, Richland, Washington 99352

[2] Environmental Molecular Sciences Laboratory, Pacific Northwest National Laboratory, P.O. Box 999, Richland, Washington 99352

libor.kovarik@pnnl.gov, mark.bowden@pnnl.gov

Abstract

High temperature exposure of γ-Al_2O_3 can lead to a series of polymorphic transformations, including the formation of δ-Al_2O_3 and θ-Al_2O_3. Quantification of the microstructure in the δ/θ-Al_2O_3 formation range represents a formidable challenge as both phases accommodate a high degree of structural disorder. In this work, we explore the use of XRD recursive stacking formalism for quantification of high temperature transition aluminas. We formulate the recursive stacking methodology for modelling of disorder in δ-Al_2O_3 and twinning in θ-Al_2O_3 and show that explicitly accounting for the disorder is necessary to reliably model the XRD patterns of high temperature transition alumina. In the second part, we use the recursive stacking approach to study phase transformation during high temperature (1050 ºC) treatment. We show that the two different intergrowth modes of δ-Al_2O_3 have different transformation characteristics, and that a significant portion of δ-Al_2O_3 is stabilized with θ-Al_2O_3 even after prolonged high-temperature exposures. In discussions, we outline the limitation of the current XRD approach and discuss a possible multimodal XRD and NMR approach which can improve analysis of complex transition aluminas.

1. Introduction

Transition aluminas represent an important group of materials that are used in a number of technological fields. For example, transition aluminas are prominently used as catalysts and catalytic supports [1-3]. In an effort to rationalize the attractive properties of transition aluminas, and ultimately understand how the properties can be tailored for specific catalytic applications, significant research efforts have focused on understanding the crystallography, structure and surfaces of transition aluminas [4-7]. For transition alumina derived from heat treatment of boehmite, the microstructure is conventionally described in terms of γ-, δ- and θ-Al_2O_3. The microstructure consists of γ-Al_2O_3 if obtained from heat treatments below ~700-800ºC [4]. At higher heat treatment temperatures, above 800 ºC, the structure topotactically reorders to structural forms of δ- and θ-Al_2O_3 [4, 8].

The formation and stability of transition alumina phases are actively studied topics. It is generally well established that the formation of δ-Al_2O_3 requires less thermal activation, while θ-Al_2O_3 is more stable and is the preferred type at higher temperatures of ~950-1000 ºC where kinetic factors play smaller roles [4]. Consequently, the formation of δ- and θ-Al_2O_3 has been conventionally expressed in terms of heat treatment temperature [4, 9]. While this provides a useful conceptual view, it is now realized that such description may not satisfactorily capture the complexity of the evolving microstructures. Both δ-Al_2O_3 and θ-Al_2O_3 can coexist in a common microstructure over a broad temperature range and, moreover, the evolving structures can represent an intermediate order state consisting of bonding environment of both δ- and θ-Al_2O_3 [10]. In addition, it has been also shown that the decomposition pathways for γ-Al_2O_3 via formation of δ-Al_2O_3 can be bypassed with a direct formation of θ-Al_2O_3. This has been demonstrated for a rod-like morphology γ-Al_2O_3 derived from boehmite [11]. As both structures of δ- and θ-Al_2O_3 have a complex crystallography and accommodate a high degree of structural disorder [10, 12, 13], reliable quantification and tracking of the microstructure as it evolves during phase transformations is the main limitation in advancing our understanding of high temperature transition aluminas.

.

Conventional XRD or NMR approaches that do not explicitly account for disorder are not well suited for structural analysis of these complex systems [7, 10, 14]. In order to address the stability and mechanism of transformations of high temperature transition aluminas, this work explores the possibility of adopting recursive stacking XRD quantification. The recursive stacking XRD techniques has been previously developed for analysis of planer disorder [15], making it thus suitable for analysis of disorder in δ/θ-Al_2O_3 microstructure. In δ-Al_2O_3, the disorder originates from the planer intergrowth of four δ_x-Al_2O_3 variants [12, 13]. In θ-Al_2O_3, there are two types of superimposed structural disorders [10]. Only one type of disorder has a planar character (twining), and is thus suitable for analysis using recursive stacking. The use recursive of stacking has been previously applied for characterization/quantification of structural intergrowth in zeolites [16], oxides [17], twined and disordered structures of SiC and kaolinite and other known planar defected structures [18].

We develop a methodology for recursive stacking in δ-Al_2O_3 and θ-Al_2O_3. and demonstrate that explicitly accounting for the disorder is necessary to reliably model the XRD patterns of high temperature transition aluminas. The developed methodology is applied to study phase transformation in high temperature transition aluminas derived from Boehmite, enabling us to describe the complexities in the evolution of δ- and θ-Al_2O_3 and their stabilities.

2. Theoretical and Experimental Description

Transition aluminas investigated in this work were obtained from dehydration of Boehmite (*Sasol*). The samples were heat treated in a tube furnace at 1050°C for a period of 2-48 hours. X-Ray Diffraction (XRD) patterns were collected utilizing a PAN analytical MPD Bragg-Brentano diffractometer equipped with Cu Kα radiation, a variable divergence slit, and a post-diffraction monochromator. Rietveld refinements of microstructure was performed using recursive stacking approach, as implemented in TOPAS 5. We use super-cell structures built by recursive stacking. The intergrowth structure of δ-Al_2O_3 contains 200 layers and 8000 atoms. The θ-Al_2O_3 contains 500 layers and 5000 atoms.

The effect of structural intergrowth on diffraction intensities for individual phases was evaluated with DIFFAX. DIFFAX is a recursive stacking simulation code developed by Treacy [15] for understanding structural intergrowth.

3. Results

3.1. High Temperature Transition Al_2O_3

We formulate the recursive stacking description of disorder in δ-Al_2O_3 and twinning in θ-Al_2O_3 based on crystallographic analysis of δ- and θ-Al_2O_3 provided in previous works [10, 12, 13]. The high temperature microstructure can be conceptually described in terms δ-Al_2O_3, which can have two different intergrowth modes, and θ-Al_2O_3 with two superimposed types of structural disorder. Depiction of the structural components of high temperature transition Aluminas is shown in Figure.1.

In δ-Al_2O_3, there are two types of intergrowths. The first type is labeled as $\delta_{1,2}$-Al_2O_3, and as suggested by the notation, the intergrowth consists of δ_1- and δ_2-Al_2O_3 variants. The variants are structurally very similar. Subtle differences between these two variants can be identified based on the population of different subsets of Al sublattice vacant/octahedral/tetrahedral sites. High degree of similarity enables high degree of structural intergrowth. The second type intergrowth is labeled as $\delta_{2,3,4}$-Al_2O_3, and it originates from δ_2-, δ_3- and δ_4-Al_2O_3 variants. All three variants are based on identical structural unit, which is stacked according to different rules. Different translational and rotational operators applied in stacking of the basic structural unit differentiate the variants. Detail account of intergrowth structure of δ_2-, δ_3- and δ_4-Al_2O was provided in Kovarik et al. [13]. XRD recursive stacking approach provides an ideal method for microstructure characterization of planar intergrowth in δ-Al_2O_3.

The structure of θ-Al_2O_3 accommodates two superimposed types of disorder, including twinning and "2D-structural" disorder. Twinning is almost exclusively restricted to (100) $_{\theta\text{-}Al2O3}$, as shown in Fig.1. It is often present in very high densities [10, 19], and thus it is an important component of θ-Al_2O_3 structure. Twining represents a planar fault,

and XRD recursive stacking approaches provide an ideal way of capturing and quantifying its extent.

On the other hand, 2D structural disorder does not have planar character, and cannot be modeled with recursive stacking approaches. Other more generic approaches, such as Debey scattering equation would be appropriate to account for this disorder [20]. Given the current limitation of implementing 2D structural disorder, the present study treats θ-Al_2O_3 as an ideal structure of β-Ga_2O_3, which has 50% octahedral and 50% tetrahedral Ga^{3+} ions. This is an approximation of θ-Al_2O_3, which is expected to have 43%-48% of tetrahedral Al^{3+} [10].

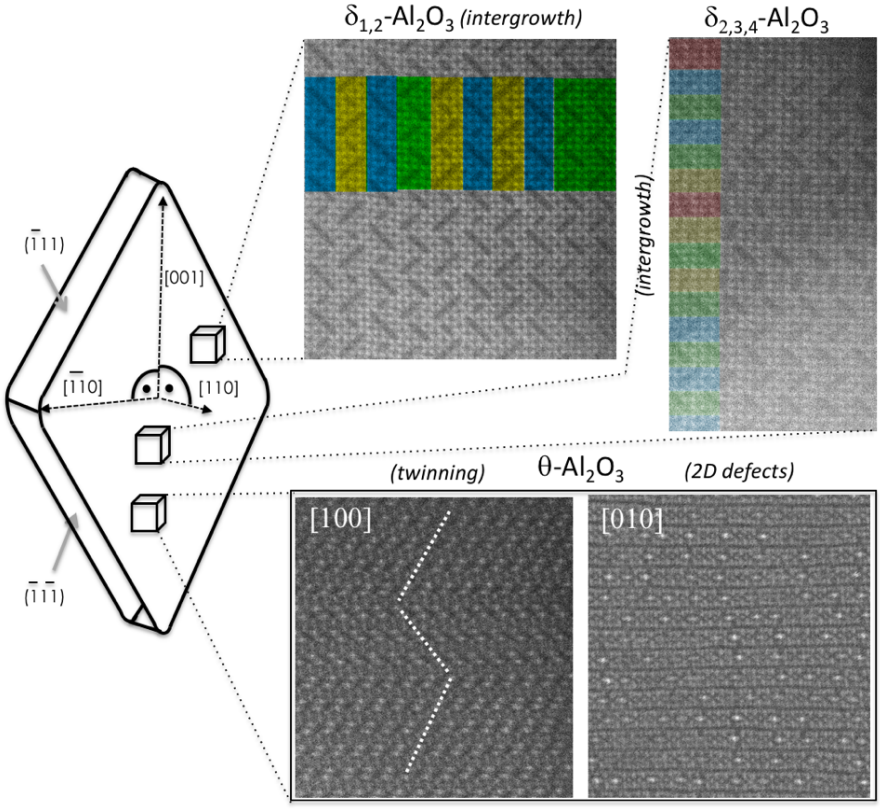

Figure.1. Schematic representation of the components of transition Alumina in δ/θ-Al_2O_3 stability region.

3.2. Methodology of Modelling Intergrowth/Twinning

3.2.1. Model of Intergrowth in $\delta_{1,2}$-Al_2O_3

Intergrowth in $\delta_{1,2}$-Al_2O_3 is formulated as recursive stacking of four layers. As shown in Fig. 2, two layers are derived from δ_1-Al_2O_3, and two layers are derived from δ_2-Al_2O_3. For the two layers derived from δ_1-Al_2O_3, each layer corresponds to half of the unit cell, as shown in Fig. 2. For the two layers derived from δ_2-Al_2O_3, each represents a full unit cell of δ_2-Al_2O_3, but they are related by 180° rotation, in order to accommodate the structure with δ_1-Al_2O_3 segments. As shown in Fig. 2, the lattice correspondence between the layers from variants of δ_1-Al_2O_3 and δ_2-Al_2O_3 can be expresses as $[001]_{\delta 1}//[010]_{\delta 2}$ and $[010]_{\delta 1}//[001]_{\delta 2}$.

All four layers in the recursive stacking have been translationally aligned with respect to each other to meet the stacking constrains, and the recursive stacking scheme itself does not require any additional translation offset. The rules for stacking of individual layers and creating intergrowth structures under the probability of occurrence for each variant are listed in Table 1. For example, layer 1, which represent δ_1-Al_2O_3 component, can only be followed by layer 2 (δ_1-Al_2O_3) or by layer 4 (δ_2-Al_2O_3). The proportion of δ_1-Al_2O_3 is controlled by probability value (δ_1%), and δ_2-Al_2O_3 by probability value $\delta_2\% = (100-\delta_1\%)$.

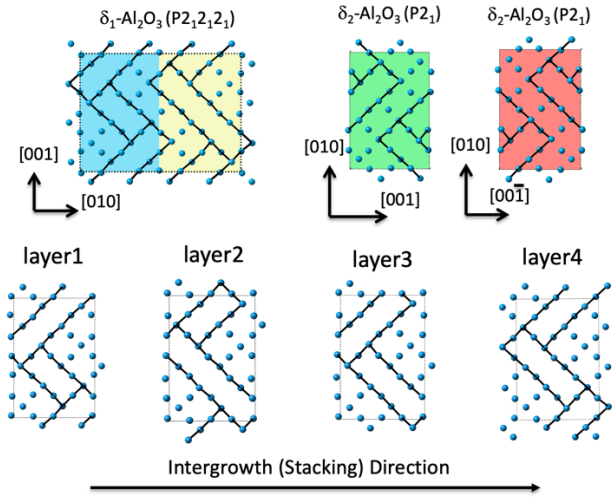

Figure.2. Formulation of structural intergrowth of δ_1-Al_2O_3 and δ_2-Al_2O_3. The structure is built by four layers, which represent the individual components of δ_1-Al_2O_3 and δ_2-Al_2O_3.

Table.1. Stacking sequence rules for formation of the intergrowth structure of $\delta_{1,2}$-Al_2O_3. The value of δ_1% represents volume fraction of δ_1-Al_2O_3.

	Layer 1 (x+1)	Layer 2 (x+1)	Layer 3 (x+1)	Layer 4 (x+1)
Layer 1 (x)	-	δ_1%	-	δ_2%
Layer 2 (x)	δ_1%	-	δ_2%	-
Layer 3 (x)	-	δ_1%	δ_2%	-
Layer 4 (x)	δ_1%	-	-	δ_2%

3.2.2. Model of Intergrowth in $\delta_{2,3,4}$-Al_2O_3

Intergrowth in $\delta_{2,3,4}$-Al_2O_3 is formulated as recursive stacking of eight layers. Each layer is structurally identical but under different rotational and translation orientation. The way the layers are related to the individual variants of δ_x-Al_2O is shown in Fig. 3. Each layer represents a half-unit cell from either of the three variants of δ_x-Al_2O_3, as shown in Fig.3.

The rules for stacking of individual layers in the intergrowth is listed in Table 2. The sequence of layers for the individual variants in the intergrowth is defined by probability δ_x%. For example, δ_2-Al_2O is obtained from recursive stacking of layers 1→2, 2→1 or 3→4, 4→3 and defined by probability δ_2%. Unlike in the previous case of $\delta_{1,2}$-Al_2O_3, the recursive stacking in $\delta_{2,3,4}$-Al_2O_3 requires that the layers are translationally aligned during recursive stacking. Additional value of required translational offset among the layers is included in Table 2.

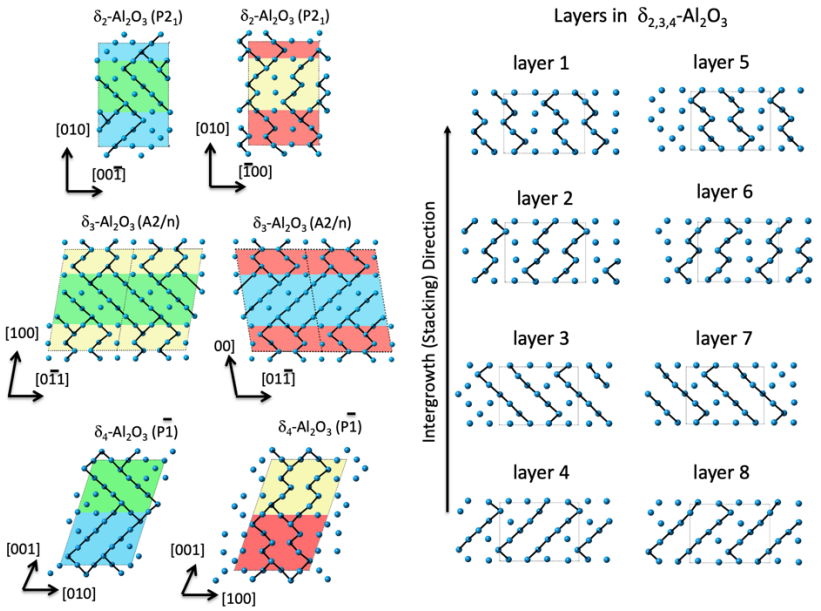

Figure.3. Formulation of structural intergrowth of δ_2-, δ_3- and δ_4-Al_2O_3. The structure is built by eight layers.

Table.2. Stacking sequence rules intergrowth structure of $\delta_{2,3,4}$-Al_2O_3. The value of δ_2%, δ_3%, δ_4% represents the fraction of δ_2-Al_2O_3, δ_3-Al_2O_3 and δ_4-Al_2O_3. The layers 5^*, 6^*, 7^*, 8^* are identical with layers 1, 2, 3, 4 but with the origin displaced by [0.5,0.5].

	Layer 1 (x+1)	Layer 2 (x+1)	Layer 3 (x+1)	Layer 4 (x+1)	Layer 5^* (x+1)	Layer 6^* (x+1)	Layer 7^* (x+1)	Layer 8^* (x+1)
Layer 1 (x)	-	δ_2% *R=[0,0]*	-	δ_3% *[-0.25,0.25]*	-	δ_4% *[0,0]*	-	-
Layer 2 (x)	δ_2% *[0,0]*	-	δ_3% *[0,0]*	-	δ_4% *[0,0]*	-	-	-
Layer 3 (x)	-	δ_3% *[0.25,-0.25]*	-	δ_2% *[0,0]*	-	-	-	δ_4% *[0,0]*
Layer 4 (x)	δ_3% *[0,0]*	-	δ_2% *[0,0]*	-	-	-	δ_4% *[0,0]*	-
Layer 5^* (x)	-	100% *[0.5,0.5]*	-	-	-	-	-	-
Layer 6^* (x)	100% *[0.5,0.5]*	-	-	-	-	-	-	-
Layer 7^* (x)	-	-	-	100% *[0.5,0.5]*	-	-	-	-
Layer 8^* (x)	-	-	100% *[0.5,0.5]*	-	-	-	-	-

3.2.3 Model of twinning in θ-Al_2O_3

Twining in θ-Al_2O_3 can be formulated relatively simply as recursive stacking of two layers. The two layers are related by mirror symmetry plus translation operation. As shown in Fig. 4, the layers are defined in terms of orthorhombic lattice, with 10 atoms in the layer, which is half the size of conventional θ-Al_2O_3 unit cell. Atomic coordinates were derived from a supercell in twinned configuration based on ab-initio calculations.

The rules for recursive stacking sequence are listed in Table 3. The transition from layer 1 to layer 1 corresponds to not-twinned configuration, while transition from layer 1 to layer 2 correspond to twin configuration, defined by the probability value (twin%). Translational offsets among the layers is required to accomplish stacking as reported in Table.3.

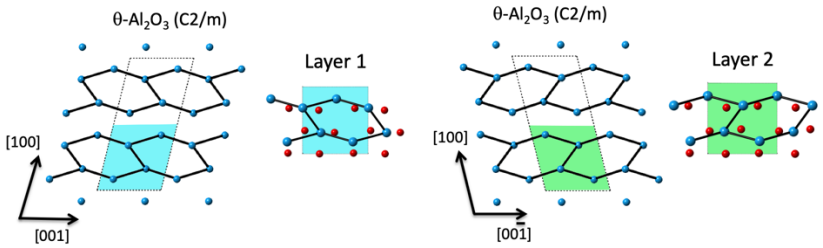

Figure.4. Formulation of twining in θ-Al_2O_3. The twin structure is built by recursive stacking of two layers.

Table.3 Rules for stacking formation of twinning in θ-Al_2O_3.

	Layer 1 (x+1)	Layer 2 (x+1)
Layer 1 (x)	(100-twin)% *R=[-0.25,0.5]*	twin% *R=[-0.25,0.5]*
Layer 2 (x)	twin% *R=[0.25,0.5]*	(100-twin)% *R=[0.25,0.5]*

3.3. The choice of refining parameters

As follows from the description above, the basic structural parameters to represent high temperature transition alumina are the volume fraction of individual intergrowth components V%($\delta_{1,2}$-Al_2O_3), V%($\delta_{2,3,4}$-Al_2O_3) and V%(q-Al_2O_3), and the level of intergrowth in each component $\delta_{1,2}$-Al_2O_3 (δ_1%,δ_2%), $\delta_{2,3,4}$-Al_2O_3 (δ_2% ,δ_3%, δ_4%) and θ-Al_2O_3 (twin%). Additional basic parameters include lattice parameters of the individual components, crystal size, as well as atom position within the structures, occupancy, Debye-Waller factor, intergrowth dilatation.

The parameter space to be derived/refined for high temperature transition aluminas is relatively large, and resolving such high number of parameters is not guaranteed with XRD. To investigate how sensitive XRD is with respect to the different intergrowth/twining in δ- and θ-Al_2O_3, the individual intergrowth/twining modes were first evaluated independently in order to understand the effect on diffraction intensities. The simulations were performed using DIFFAX software package [15]. Summary from DIFFAX simulations for the key intergrowth configurations is shown in Fig. 5. In the case of $\delta_{1,2}$-Al_2O_3, we find that changing the proportion of intergrowth parts of δ_1% and δ_2% does not have a significant effect on the main diffraction intensities. Only relatively small differences are observed for

diffraction intensities in the low two-theta region, as shown in Fig. 5a. Given the expected presence of other components, analysis of intergrowth in $\delta_{1,2}$-Al_2O_3 is not well suited for XRD refinement. In the case of $\delta_{2,3,4}$-Al_2O_3, we find that changing the proportion of intergrowth parts can have a significant effect on the main diffraction intensities. This is especially the case for intergrowth components of δ_2- to δ_3-Al_2O_3. As shown in Fig. 5b, increasing the proportion of δ_3-Al_2O_3 within δ_2-Al_2O_3 significantly modifies the relative peak intensities in the range of 30-40 º with respect to the diffraction planes in 46-47º range. This is not the case for components $\delta_{2,4}$ Al_2O_3 (Fig. 5c), where the intergrowth has only a negligible effect on the diffraction intensities. Analogously to $\delta_{1,2}$-Al_2O_3, only low intensities at relatively low diffraction angles are affected. For θ-Al_2O_3, we find that twinning has a strong effect on the relative intensities, as shown in Fig. 5d). Some of the most significant effects are observed for diffraction planes (40-1) and (111), as highlighted with arrows.

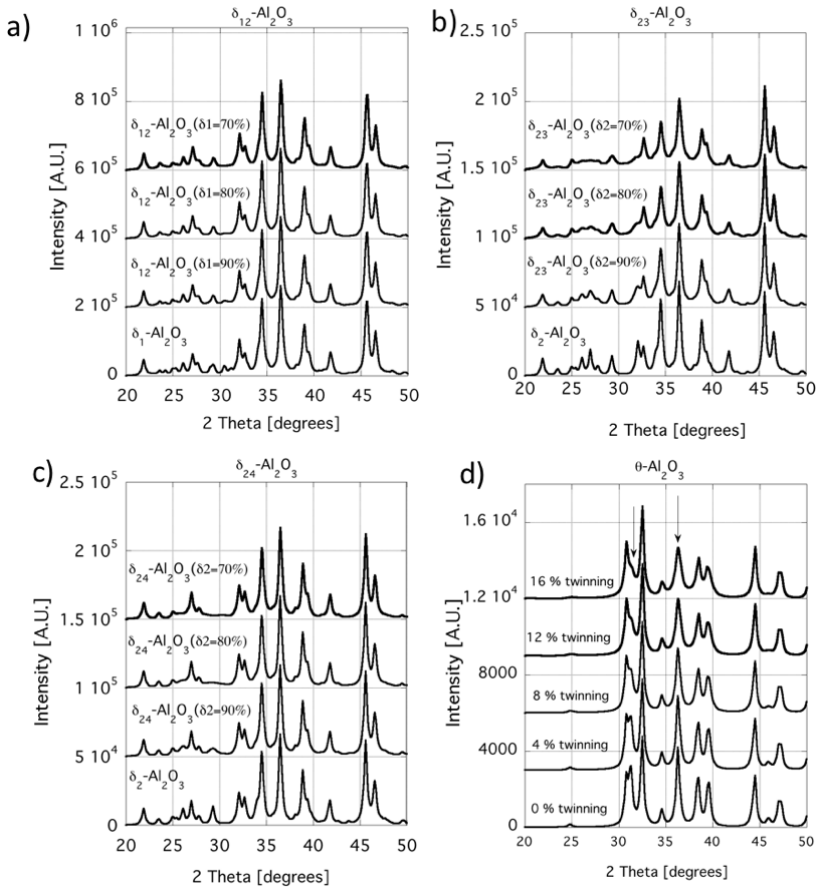

Fig. 5. DIFFAX simulated diffraction patterns for the intergrowth structures of (a) $\delta_{1,2}$-Al_2O_3, (b) $\delta_{2,3}$-Al_2O_3 (c) $\delta_{2,4}$-Al_2O_3 and (d) twinning in θ-Al_2O_3.

As suggested by DIFFAX calculations, some intergrowth modes result only in subtle changes in XRD intensities, and thus are poorly suitable for structural refinement using recursive stacking. This enables us to simplify the parameter space used for structural refinements. Since the intergrowth in $\delta_{1,2}$-Al_2O_3 does not have a strong effect on the diffraction intensities, the structure of $\delta_{1,2}$-Al_2O_3 is approximated by δ_1-Al_2O_3. For the structure of $\delta_{2,3,4}$-Al_2O_3, we only consider the contribution from δ_2- and δ_3-Al_2O_3, while omitting δ_4-Al_2O_3. For θ-Al_2O_3, twining is included as an important intergrowth mode in the refinement.

The summary of structural parameters refined in this work are indicated in Table.2. This includes volume fraction, lattice parameters and domain size. Structural parameters that were kept constant include intergrowth dilation, atomic site positions, site occupancy and Debey-Waller factor. In our work atomic site positions were derived from DFT methods, site occupancy was considered 1, and Debye-Waller factor of 1.

Table. 4. Structures and their parameters used in the Rietveld refinements.

	$\delta_{1,2}$-Al_2O_3	**$\delta_{2,3,4}$-Al_2O_3**	**θ-Al_2O_3**
Volume fraction	YES	YES	YES
Planar disorder model (intergrowth)	NO δ_1-Al_2O_3	ONLY $\delta_{2,3}$-Al_2O_3	YES twinning
Lattice parameters	YES	YES	YES
Crystal size	YES	YES	YES
Domain Size	NO	NO	NO
Intergrowth Dilatation	NO	NO	NO
Atom positions	NO	NO	NO
Atom occupancy	NO	NO	NO
Debye-Waller Factor	NO	NO	NO

3.4. Evaluation of recursive stacking approach

The newly developed recursive stacking approach was tested for its ability to represent the experimental measurements and its ability to constrain the key microstructural parameters. The tests were performed on heat treated samples at 1050 ºC, corresponding to different stages of microstructural development.

We find that the recursive stacking formalism provides an important improvements over conventional refinement. An example of XRD pattern corresponding to microstructure heated for 8h @1050 ºC is shown in Fig.6. As evident from the small residual intensity plotted in Fig 6, the recursive stacking formalism fits the relative intensities well with the merit value R of 9.5. In comparison, refining the structure using conventional linear fitting approach results in higher residual intensity and R-value 14.8, as shown in Fig. 6. This represents an improvement by factor of 1.5 for recursive stacking. A value of 10 was normally obtained in the refinement of tested microstructures. The highest R value of 10.7 was obtained for earliest stages of transformation of 2h @1050 ºC. The higher R-value is expected to originate from not accounting for the presence of small Al sublattice domains in δ-Al_2O_3 [13]. Opportunities for improving modelling of XRD pattern in the early stages of transformation are described in discussions.

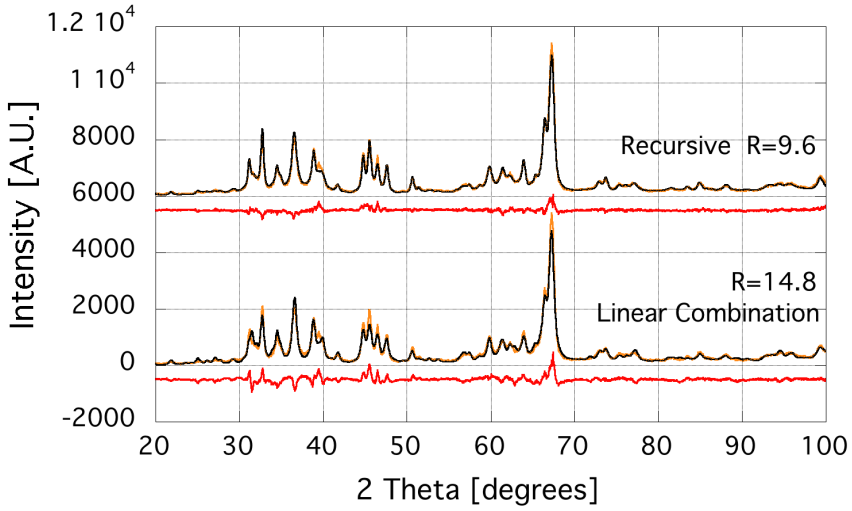

Figure.6. Comparison of XRD refinement approach based on recursive formalism and conventional formalism using a linear combination of individual phases. In both cases, the orange line represents the experimental observations and the black line represents the refinements. Red line is residual intensity.

The structural parameters defining the level of intergrowth in $\delta_{2,3}$-Al_2O_3 and twining in θ-Al_2O_3 are well constrained in the refinement. An example of parameter refinement for microstructure heat treated for 8h @1050ºC is shown in Fig.7a. The merit value (R-value) is plotted as function of structural parameters, with the global minima representing the best overall XRD fit. In this particular case we obtained the best fit when considering $\delta_{2,3}$-Al_2O_3 with 60% of δ_2 and θ-Al_2O_3 accommodating 14% of twining. The values are well constrained under the majority of tested heat treatment conditions, but the uncertainty for derived values of intergrowth/twinning parameters increases with the decreasing volume fraction of the individual component. For example, for a long calcination times, when $\delta_{2,3,4}$-Al_2O_3 is present in low volume fraction of approximately 25%, the error in estimation of intergrowth parameter become larger, as shown in Fig. 7(b). It is likely that this approach may not be well suited for refining intergrowth/twining parameters if the volume fraction of the component is less than 10%.

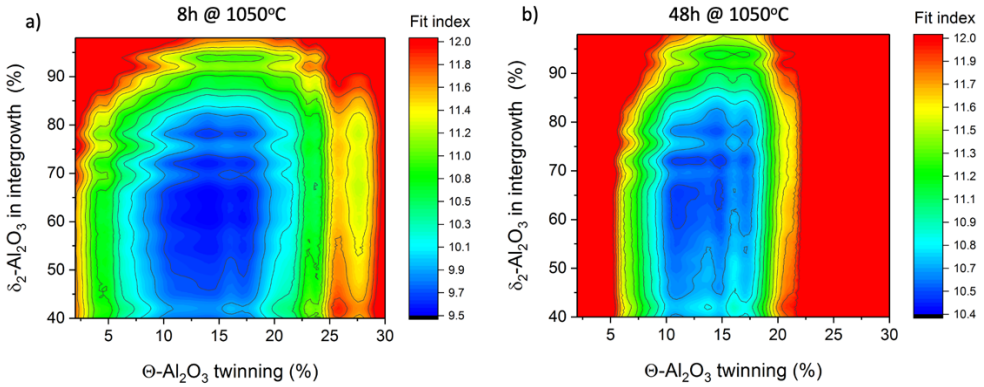

Figure.7. Refinement of structural disorder in $\delta_{2,3}$-Al_2O_3 and θ-Al_2O_3 for sample heat treated (a) 8h at 1050 ºC (b) 48h at 1050 ºC.

3.5. Application for quantification of transition Aluminas

The recursive stacking refinement was applied to study the mechanism and kinetics of phase transformation for microstructures treated for 2-48 h at 1050 ºC. In this time and temperature range, combination of $\delta_{1,2}$-, $\delta_{2,3,4}$- and θ-Al_2O_3 represent the only possible

components of microstructure. γ-Al_2O_3 can be excluded as the heat treatment extends beyond its stability range, and α-Al_2O_3 formation was not observed.

The derived volume fraction of individual components as a function of calcination time is plotted in Fig. 8(a). We find that $\delta_{2,3,4}$-Al_2O_3 is the main component forming in the microstructure in the earliest stages of aging. After 2 hours of aging, it represents approximately 65% of the total volume fraction. The remaining fraction of the microstructure corresponds to θ-Al_2O_3 rather than $\delta_{1,2}$-Al_2O_3. θ-Al_2O_3 is almost at 30% while $\delta_{1,2}$-Al_2O_3 was found only at approximately 5%. Upon continuous heat treatment at 1050 ºC, $\delta_{2,3,4}$-Al_2O_3 gradually transforms to θ-Al_2O_3 and $\delta_{1,2}$-Al_2O_3, as shown in Fig 8a. After 48hrs/1050ºC, which is the longest time presently studied, θ-Al_2O_3 is the main component, at approximately 60%, while $\delta_{2,3,4}$-Al_2O_3 decreases to approximately of 25% and $\delta_{1,2}$-Al_2O_3 increases to approximately 15%.

The key takeaways from these observations is that the two intergrowth modes of δ-Al_2O_3 have very different evolution profile. The intergrowth of $\delta_{2,3,4}$-Al_2O_3 is present in the early stages while $\delta_{1,2}$-Al_2O_3 forms as a consequence of $\delta_{2,3,4}$-Al_2O_3 transformation in later stages. θ-Al_2O_3 forms from $\delta_{2,3,4}$-Al_2O_3, at much higher rate than $\delta_{1,2}$-Al_2O_3. The δ- to θ-Al_2O_3 transformation significantly slows down during the course of heat treatment and after 48 hours of aging the microstructure appears to stabilized in a mixed δ-Al_2O_3/θ-Al_2O_3 state. This findings supports the view that both δ-Al_2O_3 and θ-Al_2O_3 can coexist in a common microstructure over a broad temperature/time range [10].

During the course of heat treatment, the level of intergrowth in $\delta_{2,3}$-Al_2O_3 or twining in θ-Al_2O_3 is found to change only to a small degree, as shown Figure8(b). The $\delta_{2,3}$-Al_2O_3 evolves towards higher proportion of δ_2. It goes from approximately 60% to 72% of δ_2 in the course of entire heat treatment. The trend towards the higher fraction of δ_2-Al_2O_3 can be rationalized on the basis of slightly improved thermodynamic stability for δ_2, and also based on the fact that δ_3-Al_2O_3 can readily transform to θ-Al_2O_3 due to symmetry similarities [10]. For the structure of θ-Al_2O_3, we find that the degree of twinning stays constant throughout the course of transformation, corresponding to approximately 14%.

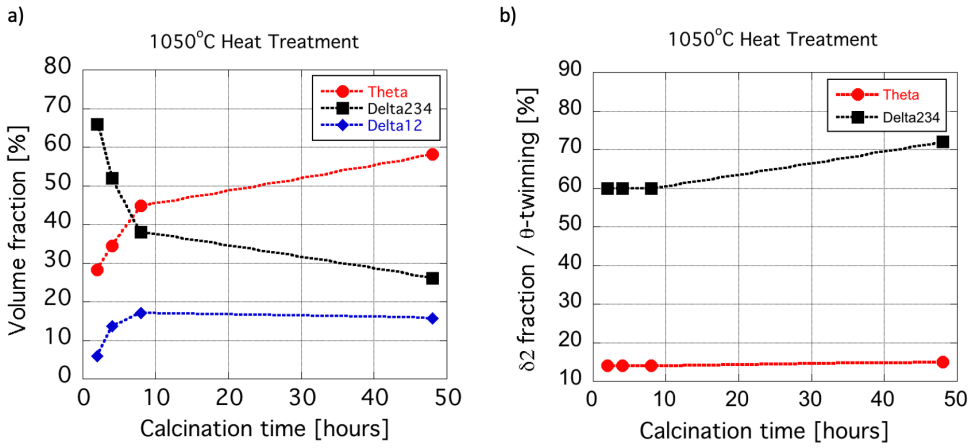

Figure. 8(a). Structural evolution of individual components of high temperature transition alumina. (b) Evolution of intergrowth disorder in $\delta_{2,3,4}$-Al_2O_3 and twining in θ-Al_2O_3.

As a part of the structural refinement, we also evaluated the lattice parameters of $\delta_{1,2}$-, $\delta_{2,3,4}$- and θ-Al_2O_3. As shown in Fig. 9, we find that the lattice parameters stay mostly constant, and within the range of experimental errors during the course of heat treatment. One of few exceptions is the lattice parameter for [100] of θ-Al_2O_3, which is found to continuously evolve towards lower values during the course of heat treatment with a total change of 0.25%. Evolution towards smaller [100] lattice parameters would be expected under the circumstances that θ-Al_2O_3 changes towards smaller amount of 2D disorder. We note that the change of 2D disorder should be also associated with an expansion of [010], but this is observed only partially. As such, judging the nature of disorder in θ-Al_2O_3 from lattice parameters is intriguing prospect but its applicability should be investigated further. In common δ-Al_2O_3/θ-Al_2O_3 microstructure, the variation in lattice parameters are also expected to be governed by coherency strains, and this may limit the utility of the approach.

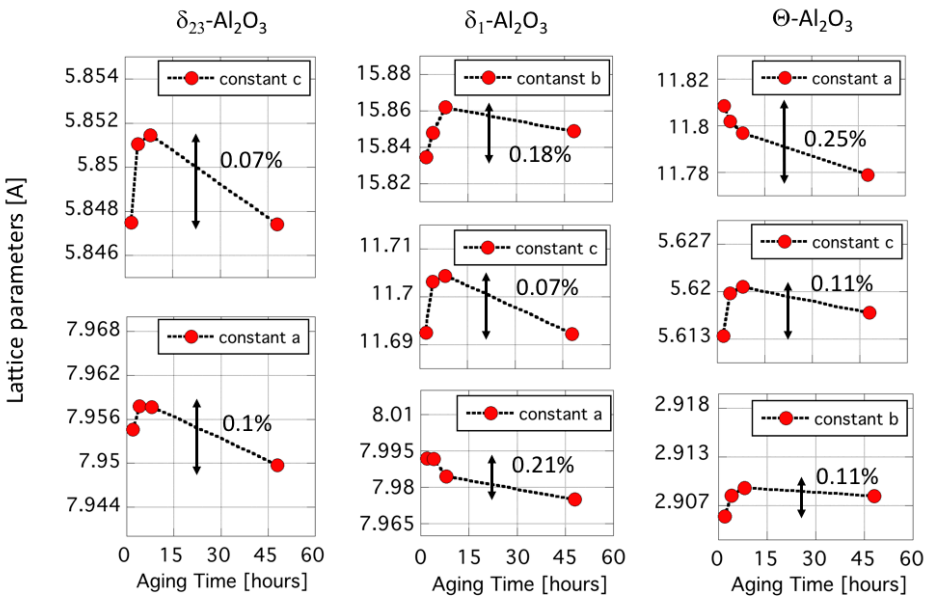

Figure. 9. Derived lattice parameters from XRD recursive refinements as a function of temperature. The lattice parameters for $\delta_{2,3,4}$-Al_2O_3 is given in terms of the basic intergrowth unit. For $\delta_{1,2}$-Al_2O_3, the lattice parameters are given in terms of orthorhombic $P2_12_12_1$ ($a \sim a_\gamma$, $b \sim 2a_\gamma$, $c \sim 1.5a_\gamma$). For θ-Al_2O_3, the lattice parameters are represented in terms of monoclinic C2/m crystal.

4. Discussion

The current work demonstrates that explicitly accounting for planar disorder in δ-Al_2O_3 and θ-Al_2O_3 is necessary to model XRD patterns of high temperature transition alumina. By accounting for the planar disorder, it is possible to derive volume fractions for individual components and their level of intergrowth/twining, which represent the key structural parameters for understanding the mechanism of phase transformations. However, the planar disorder is not the sole type of disorder found in the microstructure of high temperature. Other types of disorder are present, especially in the earlier stages of microstructure transformation. This is evident from higher values of R, which show that the planar disorder alone can no fully represent the experimentally obtained XRD spectra.

An important structural parameter, which has not been accounted in the present work, is the size of δ-Al_2O_3 and θ-Al_2O_3 domains. As schematically shown in Fig.10a, the

domains in δ- and θ-Al_2O_3 arise as a consequence of discontinuity of the Al sublattice, but with the oxygen sublattice being continuous. Physically, the discontinuity in Al sublattice can be explained with the presence of rotationally and translationally related variants of δ- and θ-Al_2O_3 sharing a common oxygen sublattice [13]. In the earlier stages of transformations, the microstructure can accommodate a high density of the domains with a size well below ~10 nm. At this small scale, subset of diffraction intensities is expected to be broadened, and accounting for the presence of domains is believed to play an important role for a reliable modelling of early stages of δ-Al_2O_3 formation. The presence of domains can be modeled using Debye scattering equation [20]. This approach has been previously applied to study the faulted structure of γ-Al_2O_3 in the work of Pakharukova et al. [7].

Another structural parameter that should be considered in the future work is the 2D disorder in θ-Al_2O_3. The disorder arises from reordering of subset of octahedral and tetrahedral sites by locally changing the bonding environment from "β-Ga_2O_3" to δ_3-Al_2O_3 like environment. Schematic of the 2D disorder and how it breaks up the long-range periodicity in 2 directions is shown in Fig. 10(b). Modelling of 2D disorder in θ-Al_2O_3 will require an algorithm for embedding 2D defects in the supercell in the presence of twining. XRD refinement is expected to require the use of Debye scattering equation. A possible alternative and simpler implementation can be envisioned by considering partial occupancies in the structure. It is noted that partial occupancies were previously considered by Zhou and Snyder [9], with a relatively high concentration of vacancies determined for both oxygen and Al sites. Provided that a correlation can be established, the use partial occupancy could provide a non-physical but a valuable alternative for easy estimation of disorder in θ-Al_2O_3.

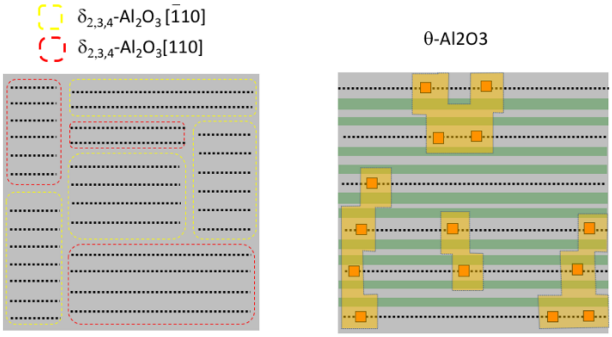

Figure.10. (a) Schematic of domain microstructure of δ-Al_2O_3 in the earlier stage. (b) schematic of 2D disorder in θ-Al_2O_3.

The high number of structural parameters needed to represent high-temperature transition aluminas raises a question whether XRD alone is suited to constrain all the parameters. Individually the parameters may be well constrained but refining the large number of parameters altogether may not lead to a unique solution. In addition, XRD also has a poor sensitivity to address some disorder types, such as the intergrowth of $\delta_{1,2}$-Al_2O_3 and δ_4 in $\delta_{2,3,4}$-Al_2O_3, as demonstrated by DIFFAX simulations. Consequently, it can be reasoned that the quantification of transition alumina may require the use of complementary techniques, ideally under global refinement. In this respect, the complementary use of NMR and XRD is especially attractive for quantification of transition aluminas. It provides an independent quantification of octahedral and tetrahedral sites, and a valuable information about the local bonding environment of Al due to the sensitivity of quadrupole nuclear magnetic moment of ^{27}Al [21, 22].

Complementary use of NMR and XRD has been previously applied for quantification of 2D disorder in θ-Al_2O_3 [10]. Since the amount of 2D disorder is directly linked to the ratio of octahedral/tetrahedral sites in θ-Al_2O_3, it was shown that the amount of 2D disorder in θ-Al_2O_3 can be directly quantified from NMR [10]. In δ-Al_2O_3/θ-Al_2O_3 microstructure, the analysis can be accomplished only if volume fraction of individual phases is determined, such as from XRD measurements. In the previous work [10], the XRD quantification used a simple model for θ-Al_2O_3 and did not account for 2D disorder. Provided that 2D disorder is implemented for XRD pattern modelling, it can be envisioned that derivation of both 2D disorder and volume fraction can be done in a combined iterative fashion for improved accuracy and reliability.

One key assumption in the analysis of 2D disorder and volume fraction is that δ-Al_2O_3 contain a known percentage of tetrahedral sites, which is 37.5%. In the earlier stages of aging (such as 2 h aging), however, making this assumption may not be justified as δ-Al_2O_3 undergoes development. It can be shown that if 37.5% of tetrahedral sites was adopted for δ-Al_2O_3, the corresponding number of tetrahedral sites in θ-Al_2O_3 would have to drop to

unrealistically low value of 39%, as shown in Fig. 9(a). It is more realistic to consider that δ-Al_2O_3 can accommodate a smaller than 37.5% of tetrahedral sites, which would then increase the tetrahedral sites in θ-Al_2O_3. In the early stages, a small change in tetrahedral sites in δ-Al_2O_3 can strongly increase the percentage of tetrahedral sites in θ-Al_2O_3. The physical origin for the modification of tetrahedral/octahedral ratio in δ-Al_2O_3 is not known, but the presence of defects, such as domain boundaries, can be hypothesized as the origin for the modification. A plausible range for the evolution of tetrahedral sites in δ-Al_2O_3 and θ-Al_2O_3 is shown in Fig 9(a). More rigorous derivation is expected to be possible based on quantitative multimodal refinements.

Quantification of transition alumina can be also pursued on the basis of NMR chemical shift and line shape anlysis [21, 22]. The non-spherical charge distribution around the ^{27}Al nucleus gives rise to a quadrupole moment. The broadening instigated by ^{27}Al's quadrupolar nature coupled with sites in somewhat similar spectral positions greatly complicates quantification of ^{27}Al species in mixtures of transition alumina phases; however, the unique chemical shifts and line shape parameters which account for the differences in the local bonding environment of alumina species and can be exploited for rigorous quantification of the overlapping broad features if they could be known precisely. Given the fact that both δ- and θ-Al_2O_3 contain a high number of unique octahedral and tetrahedral sites (e.g. 10 unique octahedral sites for δ_1-Al_2O_3 alone), and the fact that the proportion of the components changes and evolves under contrasting heat treatment conditions, NMR features for δ- and θ-Al_2O_3 should not be considered as a one-site, effective signal if being precise. Given this complexity, one possible quantification approach is to use DFT-based calculations of the chemical shielding around the ^{27}Al nuclei to simulate the line profiles for individual δ_1-Al_2O_3, δ_2-Al_2O_3, δ_3-Al_2O_3, δ_4-Al_2O_3, and θ-Al_2O_3 components as a basis for the quantification. In Figure 11(b), we show NMR spectra previously published in our work [10] and a corresponding deconvolution fit represented as a linear combination of DFT-calculated δ_1, δ_2, δ_3, δ_4, and θ-Al_2O_3 (β-Ga_2O_3 structure) NMR profiles. In this case, the sample was heated for 48 hours at 1050 °C. The best fit was obtained for a composition comprised of δ_2=13%, δ_3=19.4 % and θ-Al_2O_3=67.6%. We find that the fraction of δ-Al_2O_3/θ-Al_2O_3 is fairly consistent with XRD results (Figure 8) while

the fraction of individual components of δ_x-Al_2O_3 differs. We note that the quality of the fit and the corresponding composition is highly sensitive to the applied line-broadening to the DFT simulations; however, the general ability to represent NMR spectra in this fashion is encouraging for future quantification. Further work on combing NMR and XRD methods for comprehensive quantification of high temperature transition aluminas is ongoing.

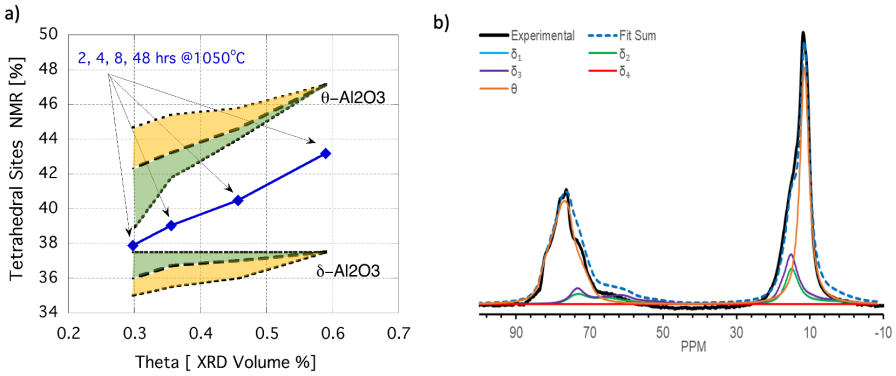

Figure. 11(a). NMR determination of the tetrahedral and octahedral sites within the structure of transition Aluminas. (b) NMR spectra of sample heated for 48 hours @ 1050 °C represented as a linear combination of δ_2, δ_3 and θ-Al_2O_3. (Lorentzian 600Hz line broadening).

In addition to NMR and XRD, there are number of other techniques that can provide unique constrains for the structure of these complex materials. It can be envisioned that multimodal approaches, ideally used under global refinement constrains, will allow for better quantification of these complex materials. Such approaches can include other techniques such as skeletal Raman spectroscopy, PDF or Neutron diffractions that have shown to provide valuable information about transition aluminas [14, 23, 24].

5. Conclusions

The current work demonstrates the utility of recursive stacking formalism for quantification of high temperature transition aluminas in δ-Al_2O_3 /θ-Al_2O_3 stability range. We find that recursive stacking approach allows to quantify the intergrowth types of δ-Al_2O_3 and θ-Al_2O_3 and its application provide a significant improvement to fit the

experimental data. The newly developed XRD refinement was applied to study the mechanism of transformation δ-Al_2O_3 to θ-Al_2O_3. It was shown that different intergrowth modes in δ-Al_2O_3 undergo different transformation pathways, and that a significant fraction of δ-Al_2O_3 remains stabilized even after prolonged exposures to high temperatures. As a part of this work, we discussed the limitation of current quantification approach, and outlined future directions for possible multimodal XRD and NMR analysis of transition Aluminas.

Acknowledgments:

This work was performed in the Wiley Environmental Molecular Sciences Laboratory (EMSL), a national scientific user facility sponsored by DOE's Office of Biological and Environmental Research and located at PNNL. This work was supported by the U.S. Department of Energy, Office of Science, Basic Energy Sciences, Chemical Sciences, Geosciences, and Biosciences Division.

References:

[1] G. Busca, The surface of transitional aluminas: A critical review, Catalysis Today, 226 (2013) 1-12.
[2] R. Wischert, P. Laurent, C. Copéret, F. Delbecq, P. Sautet, γ-Alumina: The Essential and Unexpected Role of Water for the Structure, Stability, and Reactivity of "Defect" Sites, Journal of the American Chemical Society, 134 (2012) 14430-14449.
[3] M. Trueba, S. Trasatti, γ-Alumina as a Support for Catalysts: A Review of Fundamental Aspects, European Journal of Inorganic Chemistry, 2005 (2005) 3393-3403.
[4] I. Levin, D. Brandon, Metastable alumina polymorphs: crystal structures and transition sequences, Journal of the American Ceramic Society, 81 (1998) 1995-2012.
[5] M. Digne, P. Sautet, P. Raybaud, P. Euzen, H. Toulhoat, Use of DFT to achieve a rational understanding of acid–basic properties of< i> γ</i>-alumina surfaces, Journal of Catalysis, 226 (2004) 54-68.
[6] L. Kovarik, A. Genc, C. Wang, A. Qiu, C.H. Peden, J. Szanyi, J.H. Kwak, Tomography and High-Resolution Electron Microscopy Study of Surfaces and Porosity in a Plate-like γ-Al2O3, The Journal of Physical Chemistry C, 117 (2013) 179-186.
[7] V.P. Pakharukova, D.A. Yatsenko, E.Y. Gerasimov, A.S. Shalygin, O.N. Martyanov, S.V. Tsybulya, Coherent 3D nanostructure of γ-Al2O3_ Simulation of whole X-ray powder diffraction pattern, Journal of Solid State Chemistry, 246 (2017) 284-292.

[8] S.J. Wilson, The dehydration of boehmite, γ-AlOOH, to γ-Al2O3, Journal of Solid State Chemistry, 30 (1979) 247-255.
[9] R.-S. Zhou, R.L. Snyder, Structures and transformation mechanisms of the [eta], [gamma] and [theta] transition aluminas, Acta Crystallographica, B47 (1991) 617-630.
[10] L. Kovarik, M. Bowden, D. Shi, N.M. Washton, A. Andersen, J.Z. Hu, J. Lee, J. Szanyi, J.H. Kwak, C.H.F. Peden, Unraveling the Origin of Structural Disorder in High Temperature Transition Al2O3: Structure of θ-Al2O3, Chemistry of Materials, 27 (2015) 7042-7049.
[11] J. Lee, H. Jeon, D.G. Oh, J. Szanyi, J.H. Kwak, Morphology-dependent phase transformation of γ-Al2O3, Applied Catalysis A: General, (2015) 1-11.
[12] L. Kovarik, M. Bowden, A. Genc, J. Szanyi, C.H.F. Peden, J.H. Kwak, Structure of δ-Alumina: Toward the Atomic Level Understanding of Transition Alumina Phases, The Journal of Physical Chemistry C, 118 (2014) 18051-18058.
[13] L. Kovarik, M. Bowden, D. Shi, J. Szanyi, C.H.F. Peden, Structural Intergrowth in δ-Al2O3, The Journal of Physical Chemistry C, 123 (2019) 9454-9460.
[14] G. Paglia, E.S. Božin, S.J.L. Billinge, Fine-Scale Nanostructure in γ-Al2O3, Chemistry of Materials, 18 (2006) 3242-3248.
[15] M. Treacy, J.M. Newsam, M.W. Deem, A general recursion method for calculating diffracted intensities from crystals containing planar faults, Proc. R. Soc. Lond A, 433 (1991) 499-520.
[16] T. Willhammar, X. Zou, Stacking disorders in zeolites and open-frameworks – structure elucidation and analysis by electron crystallography and X-ray diffraction, Zeitschrift für Kristallographie - Crystalline Materials, 228 (2013) 11-27.
[17] J.-R. Hill, C.M. Freeman, M.H. Rossouw, Understanding γ-MnO2 by molecular modeling, Journal of Solid State Chemistry, 177 (2004) 165-175.
[18] R.F. Giese Jr, R. Snyder, V.A. Drits, A.S. Bookin, Stacking faults in the kaolin-group minerals: Defect structures of kaolinite, Clays and Clay …, (1989).
[19] Y. Wang, P. Bronsveld, J. De Hosson, B. Djuricic, D. McGarry, S. Pickering, Twinning in theta alumina investigated with high resolution transmission electron microscopy, Journal of the European Ceramic Society, 18 (1998) 299-304.
[20] A. Leonardi, D.L. Bish, High-performance powder diffraction pattern simulation for large-scale atomistic models via full-precision pair distribution function computation, J. Appl. Cryst (2016). 49, 1593-1608 [doi:10.1107/S1600576716011729], 49 (2016) 1-16.
[21] C.V. Chandran, C.E.A. Kirschhock, S. Radhakrishnan, F. Taulelle, J.A. Martens, E. Breynaert, Alumina: discriminative analysis using 3D correlation of solid-state NMR parameters, Chemical Society Reviews, 48 (2019) 134-156.
[22] L.A. O'Dell, S.L.P. Savin, A.V. Chadwick, M.E. Smith, A 27Al MAS NMR study of a sol–gel produced alumina: Identification of the NMR parameters of the θ-Al2O3 transition alumina phase, Solid State Nuclear Magnetic Resonance, 31 (2007) 169-173.
[23] G. Paglia, C. Buckley, A. Rohl, B. Hunter, R. Hart, J. Hanna, L. Byrne, Tetragonal structure model for boehmite-derived γ-alumina, Physical Review B, 68 (2003) 144110.
[24] H.-S. Kim, P.C. Stair, Resonance Raman Spectroscopic Study of Alumina-Supported Vanadium Oxide Catalysts with 220 and 287 nm Excitation †, The Journal of Physical Chemistry A, 113 (2009) 4346-4355.